



저작자표시-비영리-변경금지 2.0 대한민국

이용자는 아래의 조건을 따르는 경우에 한하여 자유롭게

- 이 저작물을 복제, 배포, 전송, 전시, 공연 및 방송할 수 있습니다.

다음과 같은 조건을 따라야 합니다:



저작자표시. 귀하는 원저작자를 표시하여야 합니다.



비영리. 귀하는 이 저작물을 영리 목적으로 이용할 수 없습니다.



변경금지. 귀하는 이 저작물을 개작, 변형 또는 가공할 수 없습니다.

- 귀하는, 이 저작물의 재이용이나 배포의 경우, 이 저작물에 적용된 이용허락조건을 명확하게 나타내어야 합니다.
- 저작권자로부터 별도의 허가를 받으면 이러한 조건들은 적용되지 않습니다.

저작권법에 따른 이용자의 권리는 위의 내용에 의하여 영향을 받지 않습니다.

이것은 [이용허락규약\(Legal Code\)](#)을 이해하기 쉽게 요약한 것입니다.

[Disclaimer](#)

공학석사 학위논문

# 해양구조물의 동특성 평가 및 건전성 모니터링

Dynamic characteristics evaluation and structural  
health monitoring for offshore structures



지도교수 이진학  
공동지도교수 이중우

2015년 8월

한국해양대학교 해양과학기술전문대학원

해양과학기술융합학과  
정병진

공학석사 학위논문

# 해상구조물의 동특성 평가 및 건전성 모니터링

Dynamic characteristics evaluation and structural  
health monitoring for offshore structures



지도교수 이진학  
공동지도교수 이중우

2015년 8월

한국해양대학교 해양과학기술전문대학원

해양과학기술융합학과  
정병진

DYNAMIC CHARACTERISTICS EVALUATION  
AND STRUCTURAL HEALTH MONITORING  
FOR OFFSHORE STRUCTURES

BY

BYUNGJIN JUNG



The degree of Master of Science in Engineering

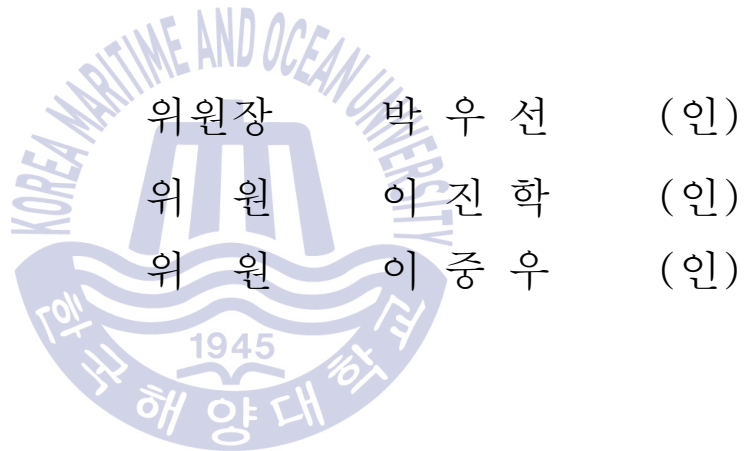
August, 2015

Department of Convergence Study on Ocean Science and Technology  
Ocean Science and Technology School  
Korea Maritime and Ocean University

Advisor Jin-Hak Yi

Co-advisor Joong Woo Lee

본 논문을 정병진의 공학석사 학위논문으로 인준함.



2015년 7월 13일

한국해양대학교 해양과학기술전문대학원

# Table of Contents

List of Tables .....	iii
List of Figures .....	iv
Abstract .....	vii

## Chapter 1. INTRODUCTION

1.1 Research Background .....	1
1.2 Literature Survey .....	3
1.3 Research Objectives and Scope .....	4

## Chapter 2. THEORETICAL BACKGROUND

2.1 Added mass .....	6
2.2 Displacement Estimation Using Data Fusion .....	8
2.2.1 Example of Displacement Estimation Algorithm .....	10
2.3 Damage index( $\beta$ ) .....	15

## Chapter 3. EXPERIMENTAL STUDY

3.1 General Information on the Lab-scale Experiments .....	18
3.2 Information on the Lab-scale Test Structure .....	20
3.3 Outline of the Lab-scale Experiment .....	25
3.4 Analysis of Experimental Results .....	27

3.4.1 Added Mass Effect .....	27
3.4.2 Boundary Damage Effect from Current Velocity Change .....	31
3.4.3 Damage Index ( $\beta$ ) .....	33
3.4.4 Displacement Estimation .....	35

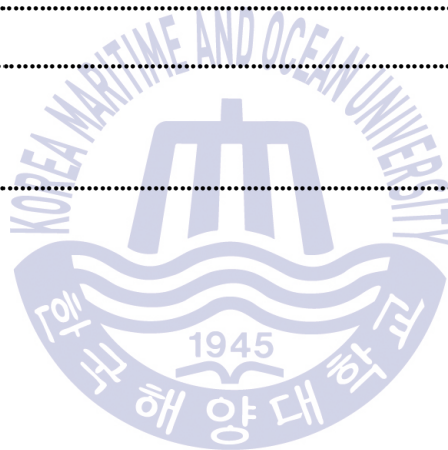
**Chapter 4. VERIFICATION OF THE EXPERIMENT**

4.1 Outline of the Numerical Modeling .....	41
4.2 Added Mass Effect .....	43

**Chapter 5. CONCLUSION**

5.1 Conclusion .....	45
5.2 Future Study .....	47

References .....	50
------------------	----



# List of Tables

<b>Table 1</b> Properties of the example model (Park et al., 2013) .....	11
<b>Table 2</b> Order of the first lab-scale experiment .....	25
<b>Table 3</b> Order of the second lab-scale experiment .....	27
<b>Table 4</b> Difference between maximum and minimum of $\beta$ for Damage case 1 and Damage Case 2 .....	35
<b>Table 5</b> Err1 and Err2 of Intact Case, Damage Case1 ,and Damage Case 2 .....	36



# List of Figures

Fig. 1.1	The first natural frequency and tidal changes of the Uldolmok tidal current power plant from September 18 to October 3, 2010 (Yi et al. 2013b) .....	2
Fig. 1.2	Previous ways and promising sensors to measuring displacement .....	3
Fig. 2.1	Displacement estimation using moving time-window (Cho et al., 2015) ...	9
Fig. 2.2	Example model - NREL 5WM wind turbine model (Park et al., 2013) ..	11
Fig. 2.3	Thrust force under top of the tower .....	12
Fig. 2.4	Real displacement form numerical analysis and displacement from using only-acceleration response of top of the tower .....	12
Fig. 2.5	Strain response on bottom of the tower and static displacement from strain response using the algorithm .....	13
Fig. 2.6	PSD data of dynamic displacement from only-acceleration and static displacement from only-strain .....	14
Fig. 2.7	Estimated displacement which is sum of dynamic displacement from acceleration and static displacement from strain, dynamic displacement from acceleration, and static displacement from strain .....	14
Fig. 2.8	Real displacement and estimated displacement .....	15
Fig. 3.1	Construction sequence in ordinary monopile foundation .....	19
Fig. 3.2	Setup for the lab-scale experiment .....	21
Fig. 3.3	Dimensions of the lab-scale test structure .....	22
Fig. 3.4	Accelerometer location and measurement direction .....	23
Fig. 3.5	Location of strain gauge covered waterproof material .....	23

<b>Fig. 3.6</b>	Camcorder setup to measure real displacement .....	24
<b>Fig. 3.7</b>	Definition of boundary conditions between the lab-scale test structure and the bottom .....	26
<b>Fig. 3.8</b>	Acceleration time history response by impact excitation (500mm water level, fore-and-aft direction) .....	28
<b>Fig. 3.9</b>	First and second bending mode shapes of the lab-scale test structure's numerical model in dry condition .....	29
<b>Fig. 3.10</b>	The first bending modal frequencies in Side-side and Fore-aft direction as water level increases .....	30
<b>Fig. 3.11</b>	The second bending modal frequencies in Side-side and Fore-aft direction as water level increases .....	30
<b>Fig. 3.12</b>	Result of the second lab-scale experiment in Damage Case 2 and its detail .....	32
<b>Fig. 3.13</b>	Changes in the first natural frequency in Intact Case, Damage Case 1, and Damage Case 2 as current velocity increases .....	33
<b>Fig. 3.14</b>	Damage index $\beta$ for Damage Case 1 and Damage Case 2 .....	34
<b>Fig. 3.15</b>	Estimated displacement at the top of the lab-scale test structure in Intact Case - first try .....	37
<b>Fig. 3.16</b>	Estimated displacement at the top of the lab-scale test structure in Intact Case - second try .....	37
<b>Fig. 3.17</b>	Estimated displacement at the top of the lab-scale test structure in Damage case 1 - first try .....	38
<b>Fig. 3.18</b>	Estimated displacement at the top of the lab-scale test structure in Damage Case 1 - second try .....	38
<b>Fig. 3.19</b>	Estimated displacement at the top of the lab-scale test structure in Damage case 2 - first try .....	39
<b>Fig. 3.20</b>	Estimated displacement at the top of the lab-scale test structure in Damage Case 2 - second try .....	39
<b>Fig. 3.21</b>	PSD data for real and estimated displacement of Damage Case 2 — first try .....	40

**Fig. 4.1** Real and simulated numerical model of the lab-scale test structures ... 42  
**Fig. 4.2** Experimental and numerical values of the first and second frequency in the fore-and-aft direction as water level increase ..... 44



# Dynamic characteristics evaluation and structural health monitoring for offshore structures

Jung, Byung Jin

Department of Convergence Study on the  
Ocean Science and Technology  
Graduate School of Korea Maritime University

## Abstract

Previous long-term measurements of the Uldolmok tidal current power plant showed that the structure's natural frequencies fluctuate with a constant cycle—i.e., twice a day with changes in tidal height and tidal current velocity. This study aims to improve structural health monitoring (SHM) techniques for offshore structures under a harsh tidal environment like the Uldolmok Strait. In this study, lab-scale experiments on a simplified offshore structure as a lab-scale test structure were conducted in a circulating water channel to thoroughly investigate the causes of fluctuation of the natural frequencies and to validate the displacement estimation method using multimetric data fusion. To this end, the numerical study was additionally carried out on the simplified offshore structure with damage scenarios, and the corresponding change in the natural frequency was analyzed to support the experimental results. In conclusion, (1) the damage that occurred at the foundation resulted in a more significant change in natural frequencies compared with the effect of added mass; moreover, the structural

system became nonlinear when the damage was severe; (2) the proposed damage index was able to indicate an approximate level of damage and the nonlinearity of the lab-scale test structure; (3) displacement estimation using data fusion was valid compared with the reference displacement using the vision-based method.

**KEY WORDS:** Structural health monitoring; Added mass; Damage detection; Displacement estimation; Tidal current power plant structure



# 해양구조물의 동특성 평가 및 건전성 모니터링

정 병 진

한국해양대학교 해양과학기술전문대학원  
해양과학기술융합학과

## 초 록

울돌목 시험조류발전소의 구조물의 고유주파수가 조위와 조류의 속도에 따라 하루에 두 번 일정한 주기로 변동하는 것을 장기적 측정을 통해 관측되었다. 울돌목과 같이 극심한 조류환경에 건설된 해양구조물의 구조물 건전성 모니터링에 관한 기술을 증진시키는 것이 본 연구의 목적이다. 울돌목 시험조류발전소의 고유주파수가 변동하는 이유를 찾고 자료융합을 이용한 변위추정알고리즘의 타당성 검토를 위해 해상구조물을 단순화한 시험체로 회류수조에서 실험실 규모의 실험을 수행하였다. 또한 손상시나리오를 시험체에 적용한 추가적인 수치해석을 실험결과를 뒷받침하기 위해 수행하였다. 결론적으로, (1) 부가질량의 효과보다는 기초지점부의 손상이 시험체의 고유주파수 변동에 더 많은 영향을 주었으며 손상이 가장 심했을 때 비선형성을 띄어 유속 즉 외력이 커짐에 따라 주파수가 변동하는 현상이 관측되었다. (2) 제안된 손상지수는 손상 정도를 나타내는 척도로써 충분하였고 비선형성 또한 나타낼 수 있었다. (3) 영상기반방법을 통해 얻어진 기준이 될 수 있는 변위와 비교를 한 결과 자료융합을 이용한 변위추정의 타당성이 입증되었다.

# CHAPTER 1

## INTRODUCTION

### 1.1 Research Background

With increasing interest in renewable energy, studies on ocean energy, such as tidal and wave energy, have been actively conducted. The Uldolmok tidal current power plant (TCPP) was built in 2009 near the Jindo Grand Bridge to develop technologies for tidal current power generation and to prepare for widespread implementation. Its performance in terms of the grid connection and power efficiency was verified (Han et al., 2013). The structure experienced difficulties during construction because the tidal current on the Uldolmok Strait has very high speeds of up to 4-5 m/s and a short tidal stand time of approximately 30 min. Therefore, there had been various attempts to maintain structural stability in this severe environment, including installing temporary loading blocks and mooring the plant with mooring chains. Also, the strain responses were measured and dynamic characteristics were monitored in the long term to secure stability in construction and maintain it effectively during operation (Yi et al., 2012). The Uldolmok TCPP's natural frequencies—one of its important dynamic characteristics—was found to fluctuate in the same period as the tidal cycle—i.e., approximately 6 hours and 12 hours, which are the periods of M4 and M2 tidal constituents, respectively. In addition, it was necessary to determine the cause of this; the first natural frequency fluctuated and varied by up to 16% in a day, which is relatively much greater than that of onshore structures, including buildings and bridges (Yi et al., 2013b). This observation was the motivation behind this

study. The first frequency, tidal current velocity, and tidal height of the Uldolmok TCPP are shown in Fig. 1.1.

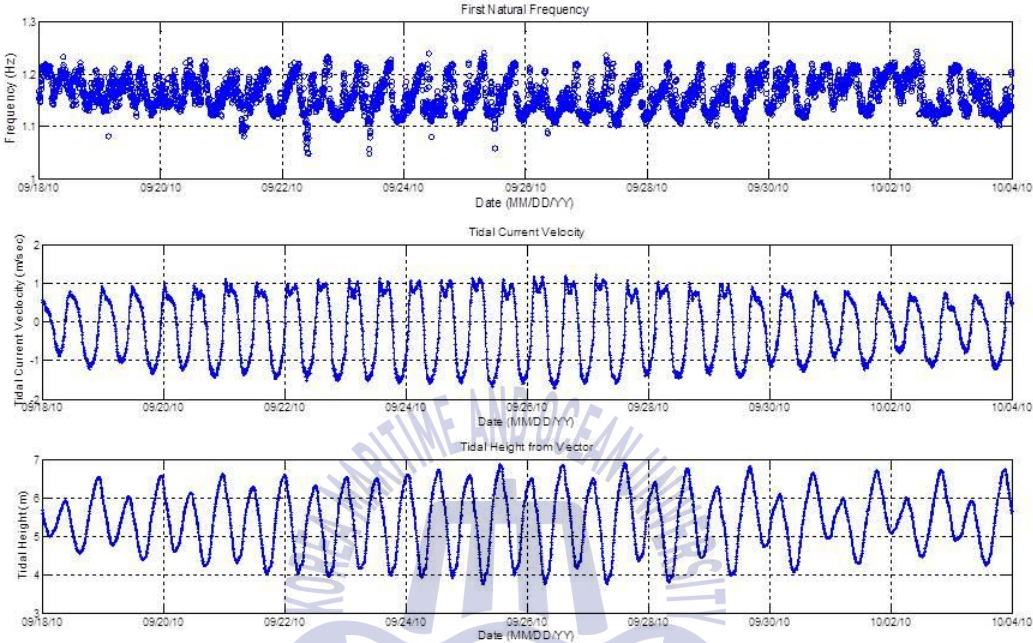


**Fig. 1.1** The first natural frequency and tidal changes of the Uldolmok tidal current power plant from September 18 to October 3, 2010 (Yi et al., 2013b)

Estimating displacement is also one of the key technologies in the structural health monitoring field. From the displacement data, we can estimate internal force like moment. Dynamic characteristics can be founded because displacement includes dynamic component. Previous method to identify dynamic characteristics is by using acceleration response. Monitoring displacement can give modal information as well as internal force information.

## 1.2 Literature Survey

The natural frequency is a typical damage factor and its change is closely related to structural damage in terms of SHM (Salawu, 1997; Kim & Stubbs 1995). Therefore, it was important to find the reason why the Uldolmok TCPP' s first natural frequency has fluctuated. Also, many studies have been carried out to estimate the damage of infrastructures using untypical methods such as modal strain energy (Huynh et al., 2013).

Displacement can also be a vital damage index (Li et al., 2014). Monitoring displacement helps us to intuitively and directly realize structure conditions, such as detecting structural damage and deformation, from the external loads.

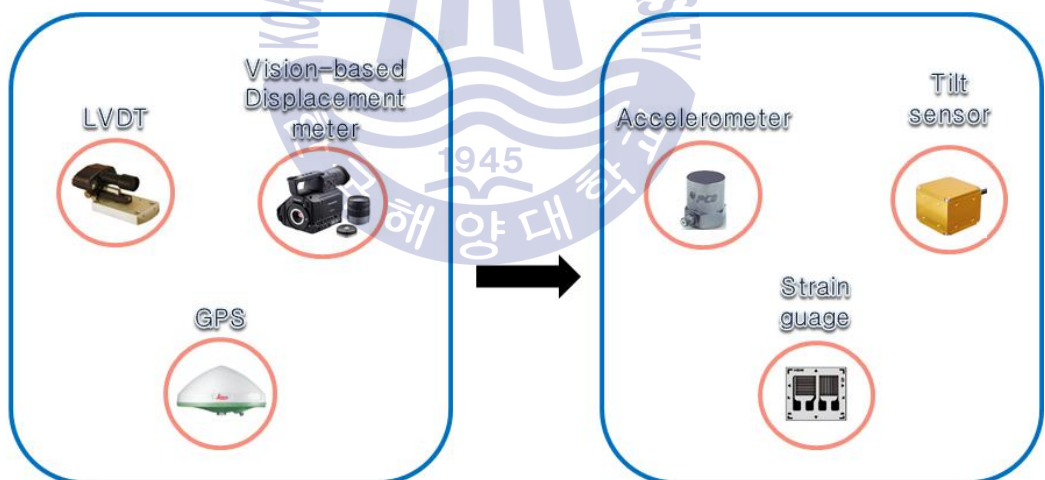


**Fig. 1.2** Previous ways and promising sensors to measuring displacement

Measuring displacement is possible with the use of several methods, including a linear variable differential transformer (LVDT), a LASER Doppler Vibrometer

(LDV) (Nassif et al., 2005), a global positioning system (GPS) (Celibi, 2000), and a vision-based displacement meter. However, these methods are not usually appropriate for offshore structures. Using an LVDT in offshore structures is impossible; it needs a fixed point to measure relative displacement. An LDV has high resolution and performance, however it is very costly. As for GPS, the resolution is too low to suitably measure displacement. A vision-based displacement meter is sensitive to weather and is limited in field applications. However, a strain gauge and accelerometer are easy to install on the structure and obtain strain and acceleration responses. Indirect displacement can be estimated economically by fusing the strain and acceleration responses. Park et al., (2013) proposed the data fusion method using strain and acceleration responses and validated these by comparing multimetric displacement from the proposed method to real displacement from a LASER displacement sensor through the field experiments' on the Sorok Bridge. Cho et al., (2014) numerically validated various types of beam structures using this method. It is necessary to conduct experiments to validate this data fusion method in cantilever beams such as those used in the monopole-type tidal turbines like MCTs (Marine Current Turbines) (Fraenkel, 2007).

### 1.3 Research Objectives and Scope

This study investigates the important issues in SHM systems for offshore structures that are generally exposed to a harsh environment with strong tidal forces. The critical issues discussed in this study include:

- Identification of dynamic behavior under the tidal current

- Damage detection tailored to offshore structures
- Displacement-based structural condition assessment

These issues are experimentally examined using a scale model in a water channel. A finite element model of the lab-scale test structure is built using ABAQUS to support the experimental results.

This thesis is written based on the author's paper titled "Issues in structural health monitoring for fixed-type offshore structures under harsh tidal environments, published in Smart Structures and System (Jung et al., 2015).



## CHAPTER 2

### THEORETICAL BACKGROUND

#### 2.1 Added Mass

Added mass literally means that added mass affecting structural dynamical response. When we consider mass of offshore structures in calculating or estimating dynamical parameters, that mass would be bigger than we expected. For example, mass of a structure added mass can be some value (mentioning below), water mass in submerged members, and living organisms on that member surface except for original mass of a structure. A tubular lab-scale test structure was used in this lab-scale experiment because many offshore structures, including the Uldolmok TCPP, consist of this kind of section. The Keulegan-Carpenter number ( $K_c$ ) in Eq. (2.1) is less than 3, the added mass ( $M_a$ ) can be written as Eq. (2.2) in the case of the cylindrical section (DNV, 2010). We assumed that mass of living organisms is negligible and water is not in submerged members. Besides, because  $K_c$  for the lab-scale test structure is lower than 3, Eq. (2.2) can be satisfied.

$$K_c = \frac{VT}{L} \quad (2.1)$$

where  $V$ ,  $T$ , and  $L$  are the amplitude of the flow or object's velocity oscillation, the period of the oscillation, and the diameter for a cylinder,

respectively.

$$M_a = \rho\pi a^2 \quad (2.2)$$

where  $\rho$ , and  $a$  are the density of fluid and radius of the cylinder section, respectively. The original formula of the  $i$ -th natural frequency is like Eq. (2.3); however, when a structure is affected by added mass, the  $i$ -th natural frequency can be calculated as Eq. (2.4).

$$f_i = \frac{1}{2\pi} \sqrt{\frac{K_i}{M_i}} \quad (2.3)$$

$$f_i = \frac{1}{2\pi} \sqrt{\frac{K_i}{M_i + M_{ai}}} \quad (2.4)$$

where  $M_i$ ,  $K_i$ , and  $M_{ai}$  are the generalized mass( $\phi_i^T M \phi_i$ ), stiffness( $\phi_i^T K \phi_i$ ), and added mass( $\phi_i^T M_a \phi_i$ ) of the  $i$ -th mode, respectively, where  $\phi_i$ ,  $M$ , and  $K$  are the mode shape matrix of the  $i$ -th mode, mass matrix, and stiffness matrix of a structure, respectively. Added mass can be influenced by the relative velocity between fluid and a structure, period of the structure, and surface roughness in a case where  $K_c$  is larger than 3. Therefore, the added mass shown in Eq. (2.2) can be considered as a simplified form for the practical design purposes.

## 2.2 Displacement Estimation Using Data Fusion

Lee et al., (2010) proposed an FIR filter using acceleration to estimate displacement. The estimated displacement can be calculated as Eq. (4), which is the analytical solution of Eq. (2.5) known as the Tikhonov regularization scheme.

$$\text{Min} \mathbf{I} = \frac{1}{2} \| L_a(L_u u - (\Delta t)^2 \bar{a}) \|_2^2 + \frac{\lambda^2}{2} \| u \|_2^2 \quad (2.5)$$

$$u_i = (L^T L + \lambda^2 I)^{-1} L^T L_a \bar{a} (\Delta t)^2 = C_a \bar{a} (\Delta t)^2 \quad (2.6)$$

where  $L=L_a L_c$  and  $C_a = (L^T L + \lambda^2 I)^{-1} L^T L_a$ , and where  $L_a$  is a diagonal weighting matrix,  $L_c$  in Eq. (2.7) is the linear algebraic operator matrix,  $\| \cdot \|_2$  is the two-norm of a vector, and  $\lambda$  in Eq. (2.8) is the optimal regularization factor, which is determined by the number of data points during the first natural period.

$$L_c = \begin{bmatrix} 1 & -2 & 1 & & & \\ & 1 & -2 & 1 & & 0 \\ & & & \ddots & & \\ & 0 & & 1 & -2 & 1 \\ & & & & 1 & -2 & 1 \end{bmatrix} \quad (2.7)$$

$$\lambda = 46.81 N_d^{-1.95} \quad (2.8)$$

where  $N_d$  is the time-window size, which is the acceleration response to be

processed into displacement. Theoretically, the acceleration can be get from the second-order derivative of displacement; however, calculated displacement in that way would be divergent without the boundary condition. In order to resolve this problem, an overlapping moving window strategy is taken as shown in Fig. 2.1.

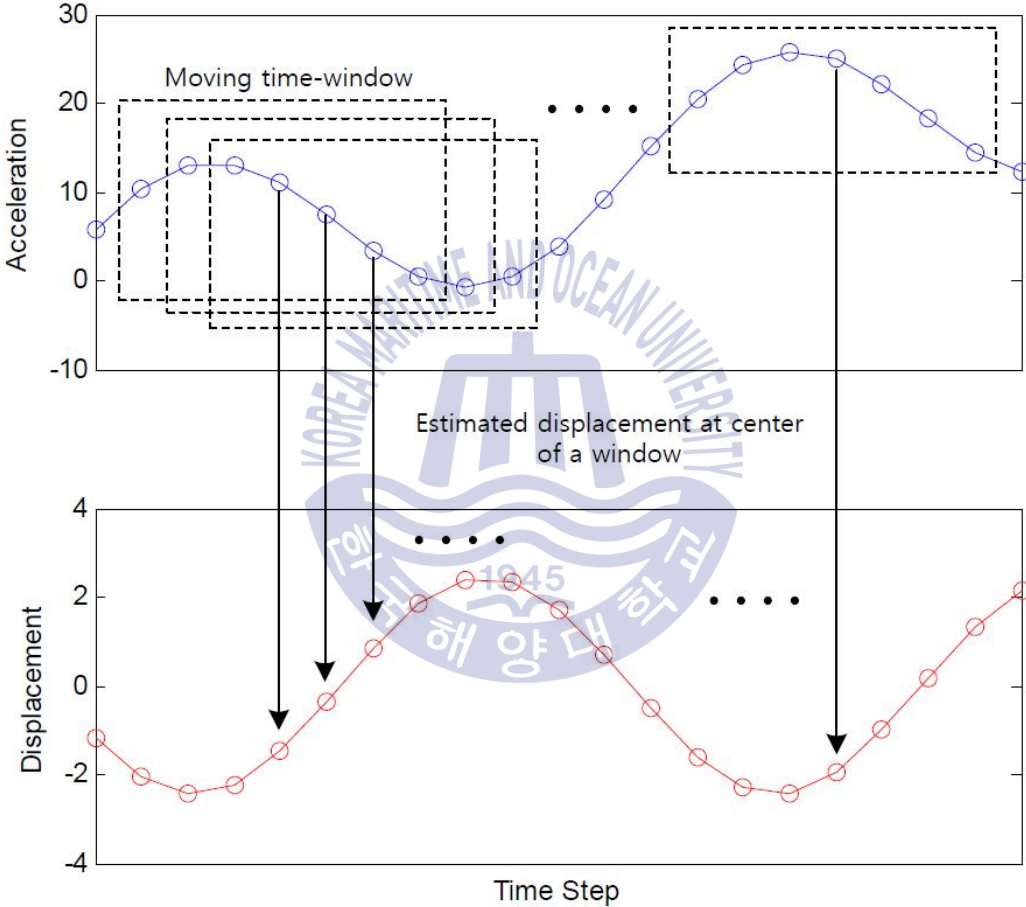


Fig. 2.1 Displacement estimation using moving time-window (Cho et al., 2015)

Detailed information on derivation can be found in Lee et al., (2010). This method is limited in estimating quasi-static displacement. Park et al., (2013) developed this method by adding the quasi-static displacement component from the strain response—the so-called data fusion in Eqs. (2.9), (2.10), and (2.11).

$$\text{Min} \prod_u = \frac{1}{2} \| L_a(L_a u_i - (\Delta t)^2 \bar{a}) \|_2^2 + \frac{\lambda^2}{2} \| u_i - D_i \bar{\epsilon} \|_2^2 \quad (2.9)$$

$$u_i = (L^T L + \lambda^2 I)^{-1} (L^T L_a \bar{a} (\Delta t)^2 + \lambda^2 \alpha D_i \bar{\epsilon}) \quad (2.10)$$

$$\begin{aligned} u_i &= [C_a^{-1} (\Delta t)^2 \quad C_\epsilon] \begin{bmatrix} a_i \\ \bar{\epsilon} \end{bmatrix} \\ &= C_a a_i (\Delta t)^2 + C_\epsilon \bar{\epsilon} \end{aligned} \quad (2.11)$$

### 2.2.1 Example of Displacement Estimation Algorithm

Displacement generally consists of dynamic displacement and static displacement. Dynamic displacement from aerodynamic and hydrodynamic force has modal information. Estimating static displacement from drag forces is important in that internal force such as bending moment and amount of external force could be find out. To understand this algorithm efficiently, one example is introduced as shown in Fig. 2.2. Unlike tidal current power plant including Uldolmok TCPP, this model represented a wind turbine is relatively simple structure and under simple external force because this structure is monopile type and governing force is thrust force on top of the wind tower.

Properties of this model are in Table 1. Figure 2.3 shows thrust force under wind tower. To distinguish dynamic and static displacement, wind load become zero after about 150 seconds. As shown in Fig. 2.4, especially in the red box, dynamic displacement of free vibration is almost same as displacement from only-acceleration after about 150 seconds. Acceleration of top of the tower and strain of bottom of the tower were measured.

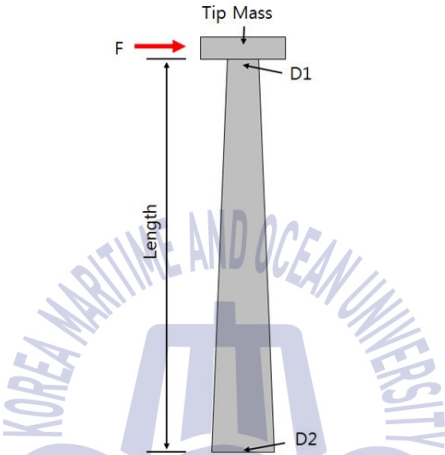


Fig. 2.2 Example model - NREL 5WM wind turbine model (Park et al., 2013)

Table 1 Properties of the example model (Park et al., 2013)

Property	Value
Length	90m
Tip Mass	350 ton
No. element	15
D1 / t1	$\Phi$ 4m / 19mm
D2 / t2	$\Phi$ 6m / 27mm
Major natural frequencies	0.33 Hz, 3.44 Hz 10.33Hz

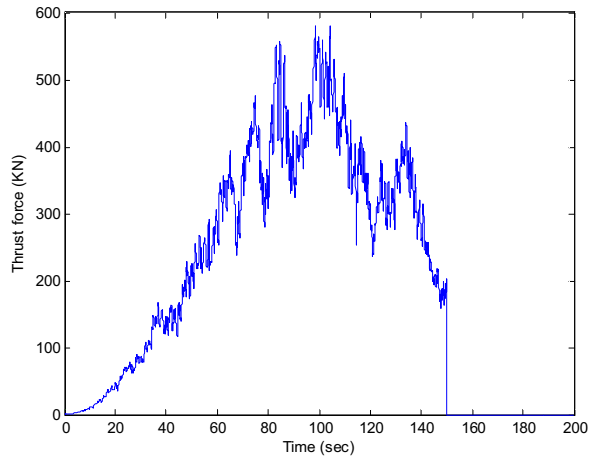


Fig. 2.3 Thrust force under top of the tower

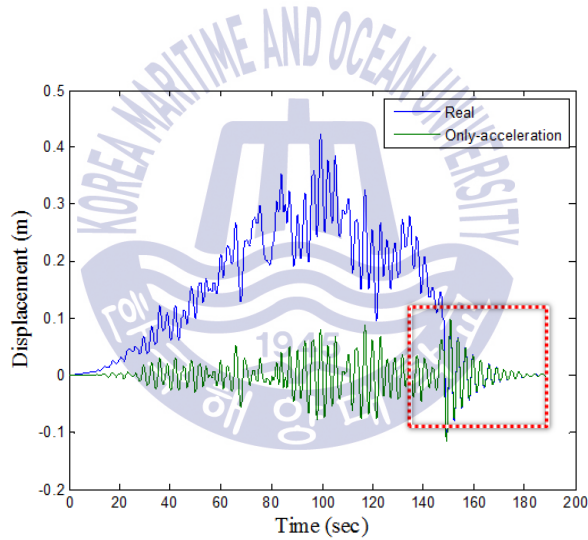
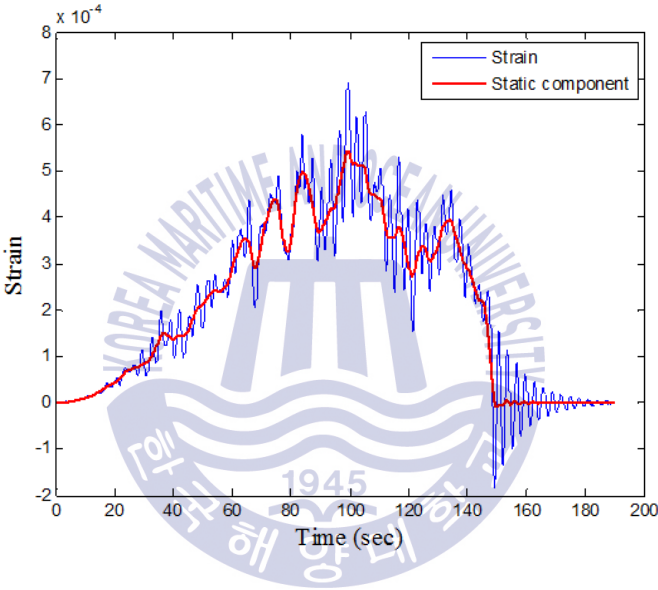


Fig. 2.4 Real displacement form numerical analysis and displacement from using only-acceleration response of top of the tower

Applying this algorithm, a graph having same trend of static displacement can be calculated from dynamic strain response like Fig. 2.5. Amplitude of

this graph is relatively small compared to Fig. 2.4, because this graph is not real static displacement but strain. To get static displacement, alpha value in Eq. (2.15) was used. Figure 2.6 shows PSD data of dynamic displacement from only-acceleration and static displacement from only-strain. Alpha is the ratio of amplitudes between the first natural frequency of displacement from only-strain and that from only-acceleration.



**Fig. 2.5** Strain response on bottom of the tower and static displacement from strain response using the algorithm

Static displacement, red line in Fig. 2.7, can be solved by multiplying alpha value and red line in Fig. 2.5. Estimated displacement in Fig. 2.7 become sum of dynamic displacement from acceleration, the green line and static displacement from strain, the red line. Figure 2.8 indicates estimated displacement and real displacement. It also shows this algorithm is valid since these are almost same.

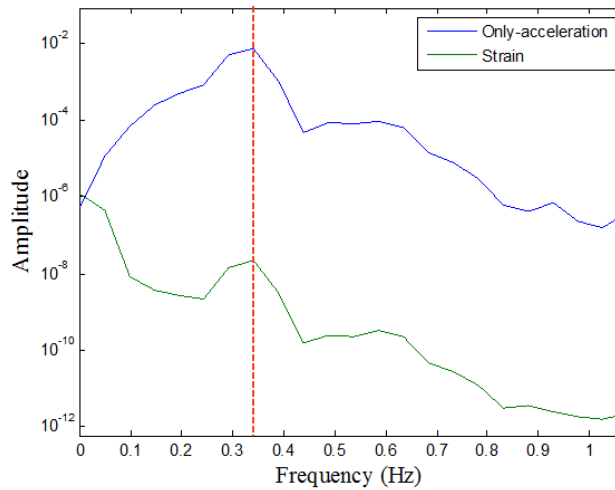


Fig. 2.6 PSD data of dynamic displacement from only-acceleration and static displacement from only-strain

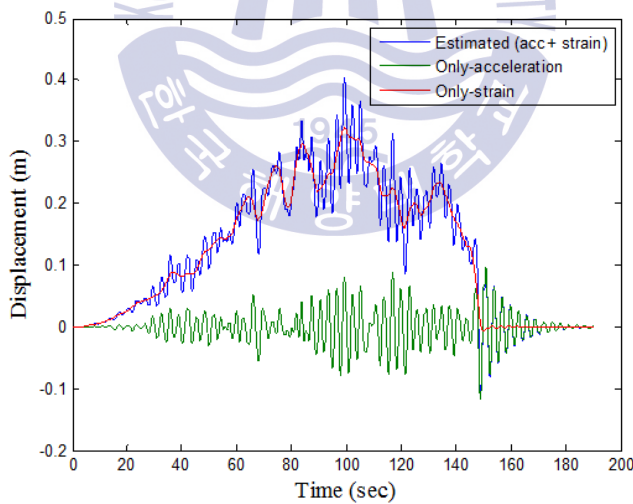


Fig. 2.7 Estimated displacement which is sum of dynamic displacement from acceleration and static displacement from strain, dynamic displacement from acceleration, and static displacement from strain

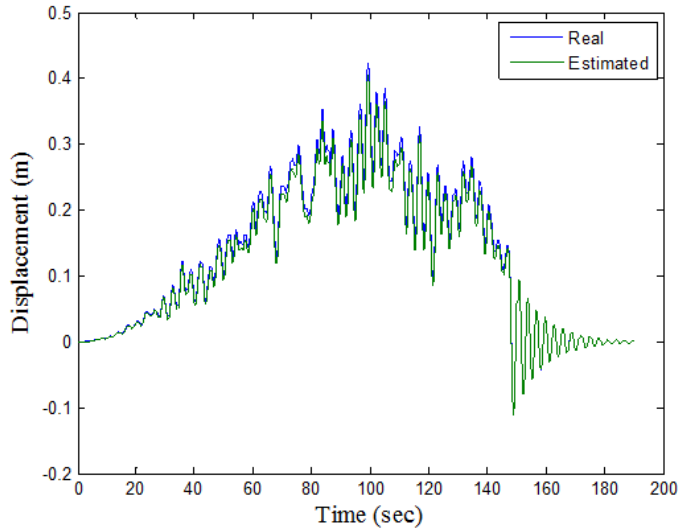


Fig. 2.8 Real displacement and estimated displacement

### 2.3 Damage Index( $\beta$ )

The displacement and strain responses in the finite number of modes  $\{u\}_{m \times 1}$  and  $\{\epsilon\}_{n \times 1}$  can be formulated by Eqs. (2.12) and (2.13).

$$\{u\}_{m \times 1} = \Phi_{M \times r} \{q\}_{r \times 1} \quad (2.12)$$

$$\{\epsilon\}_{n \times 1} = \Psi_{n \times r} \{q\}_{r \times 1} \quad (2.13)$$

where  $\Phi_{m \times r}$  and  $\Psi_{n \times r}$  are the displacement mode shape matrix and strain mode shape matrix, respectively;  $\{q\}_{r \times 1}$  is the modal coordinate;  $m$  and  $n$  are the number of measurements; and  $r$  is the number of selected modes. In  $n \geq$

r, eliminating  $\{q\}_{r \times 1}$  from Eqs. (2.12) and (2.13) yields Eq. (2.14).

$$\{u\}_{m \times 1} = \Phi_{m \times r} \Psi_{r \times n}^+ \{\epsilon\}_{n \times 1} \quad (2.14)$$

Dynamic displacement and quasi-static displacement can be theoretically obtained from Eq. (2.6) and Eq. (2.14), respectively. Estimation of dynamic displacement is quite accurate. However, it is hard to estimate quasi-static displacement; since, the neutral axis of a structure can depend on the load intensity when the structure does not have perfect symmetric structural property. We introduced the term  $\alpha$  in Eq. (2.15) in order to solve this problem.

$$\alpha = \sqrt{\frac{S_{d,acc}(f_1)}{S_{d,strain}(f_2)}} \quad (2.15)$$

where  $\alpha$  is a scaling coefficient and has a ratio of  $S_{d,acc}(f_1)$  to  $S_{d,strain}(f_1)$ .  $S_{d,acc}$  and  $S_{d,strain}$  are the power spectral densities of the displacement from acceleration and strain, respectively; and  $f_1$  denotes the first natural frequency. By multiplying Eq. (2.14) and Eq. (2.15), quasi-static displacement can be also obtained accurately as Eq. (2.16).

$$\{u\}_{m \times 1} = \alpha_{m \times m} \Phi_{m \times r} \Psi_{n \times r}^+ \{\epsilon\}_{n \times 1} \quad (2.16)$$

In addition, the term  $\alpha$  only relies on the modal property and it has a

particular value in an Intact Case; however, the presence of structural damage causes this coefficient to change. Therefore,  $\alpha$  in Eq. (2.15) can be defined as the damage index. Equation (2.17) shows damage index, which has the same base as the normalized damage factor (NDF) proposed by Park et al., (2014).

$$\beta = \left\{ \frac{\alpha_{Damage\ Case}}{\alpha_{Intact\ Case}} - 1 \right\} \times 100 \quad (2.17)$$

where  $\alpha_{Intact\ Case}$ ,  $\alpha_{Damage\ Case}$  are the scaling coefficients in Intact Case and Damage Case, respectively.



## Chapter 3.

### EXPERIMENTAL STUDY

#### 3.1 General Information on The Lab-scale Experiments

Changes in the natural frequencies are related to the mass and stiffness of structures, and they are directly connected to structural integrity; therefore, it is very important to study the cause of these changes. First, it is necessary to analyze the effect of added mass because the change of mass influences the structural system. When submerged or semi-submerged structures are vibrated in fluid, the fluid mass of the submerged portion of a structure is added to its self-weight. As a result, the natural frequency decreases and the modal damping ratio increases compared to when it is not submerged (Weiner et al., 1994; Sedlar et al., 2011; Lee et al., 2012; Lee et al., 2013). Second, temperature changes and local damages in structures can affect the stiffness of the structure and can also affect the natural frequency. Temperature changes were not considered in this lab-scale experiment on the basis of the fact that the fluctuation in the temperature of the sea—from approximately 1 to 2 ° C per day around the Uldolmok TCPP—did not greatly influence the natural frequencies. In addition, there could be difficulties with the grouting operations connecting the jacket support-structure and its foundation; even if these operations were successfully carried out, the concrete grout would be cracked by the fatigue. When construction sequence in ordinary monopile foundation was considered as shown in Fig. 3.1, cracks can cause nonlinearity in a structure.

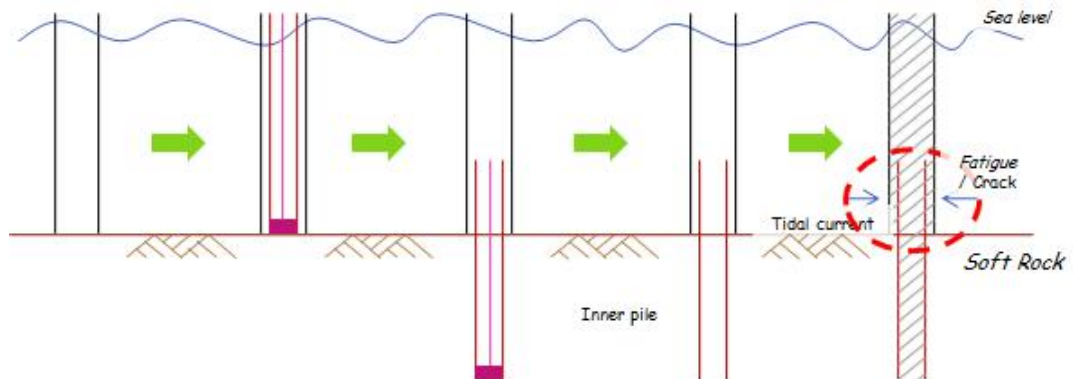


**Fig. 3.1** Construction sequence in ordinary monopile foundation

Even if the natural frequencies are independent of the applied force, we needed to examine the dynamic response with an increasing current velocity, which is the governing load for the Uldolmok TCPP. The lab-scale experiments to find the main factor that influences the natural frequencies were performed by considering that the dependent variables of the natural frequencies change as the water level changes and that the boundary damages change between the support structure and its foundation with increasing current velocity.

To verify the proposed method to estimate displacement, we needed random excitation to simulate natural conditions and to make not only dynamic displacement but also quasi-static displacement. The current can generate dynamic displacement. Quasi-static displacement was induced to maintain the current velocity. The current velocity was controlled by adjusting the valve controlling the water quantity and the sluice gate located at the end of a circulating water channel.

Therefore, three different lab-scale experiments were performed:

1. To investigate the effect of added mass on the lab-scale test structure by controlling the water level without flow;
2. To investigate how the damage levels of the lab-scale test structure affect its natural frequencies under different load conditions—i.e., by increasing the current velocity; and
3. To verify the proposed displacement estimation method by increasing, maintaining, and decreasing the current velocity.

### 3.2 Information on the Lab-scale Test Structure

The lab-scale experiments were conducted in a circulation water channel, as shown in Fig. 3.2. The circulating water channel can generate the water current uniformly and control the water level. Note that the structural behaviors of the Uldolmok TCPP have been influenced more by the tidal current than by waves. The lab-scale test structure of the Uldolmok TCPP was designed in the shape of a monopile support structure. The natural frequencies of the test structure are higher than those of the Uldolmok TCPP—unlike the original intention—because of the use of the commercially available steel pipe and the limitations in a pipe height. In general, Reynolds similarity rule can be used to evaluate the fluid-induced lift force and other related works.

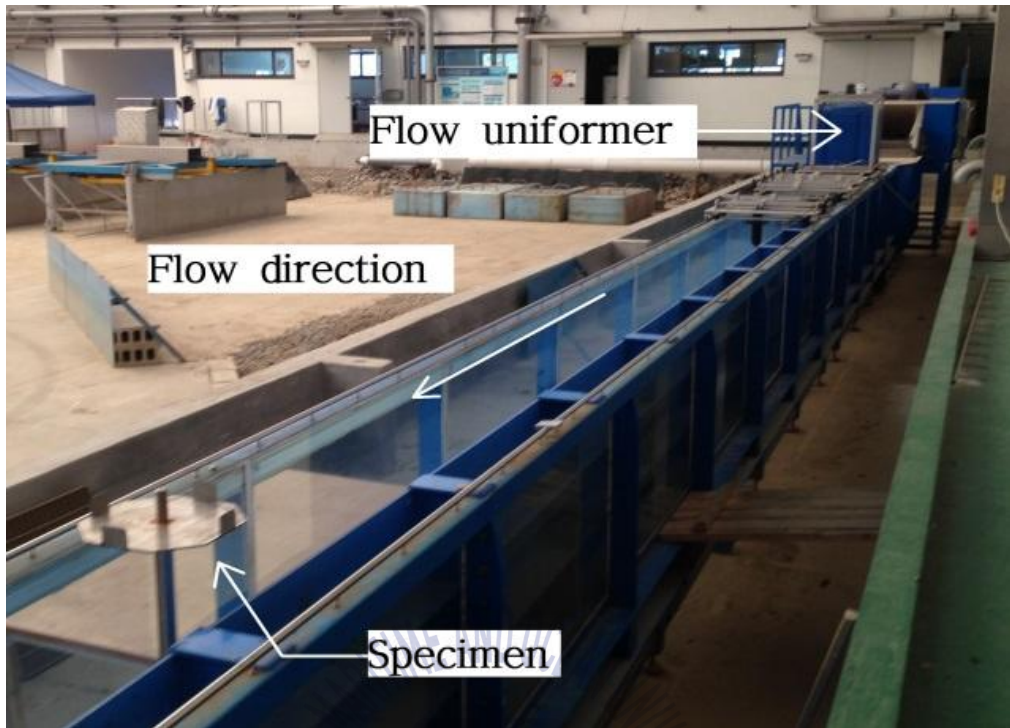


Fig. 3.2 Setup for the lab-scale experiment

Meanwhile Froude similarity rule can be applied to evaluate the wave forces on a coastal structure, such as caissons and blocks of breakwater, which are subjected to waves (Yi et al., 2013a). However, these similarity rules were not used in this lab-scale experiment; since this is beyond the scope of this study. The objective of this study is limited to analyze the effect of added mass and the stiffness of the foundation on the structural dynamic characteristics. Additional research on the Strouhal number should be conducted to analyze the vortex frequency. As shown in Fig. 3.3, the lab-scale test structure is made of stainless steel, and its height, diameter, and thickness are 1.1 m, 38 mm, and 2 mm, respectively.

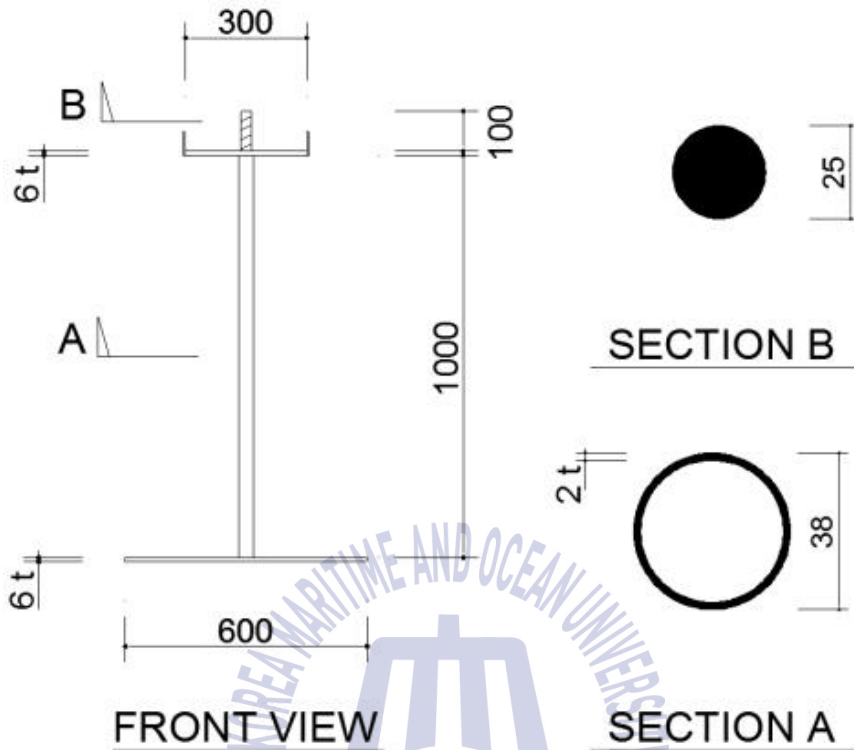


Fig. 3.3 Dimensions of the lab-scale test structure

As shown in Fig. 3.4, accelerometers were installed on the top plate to measure acceleration in the fore-and-aft and side-to-side directions, and two accelerometers in the fore-and-aft direction were used to obtain not only bending modes but also the torsional modes. The selected accelerometers are integrated circuit piezoelectric (ICP) Type 355B53, PCB Piezotronics, Inc. Strain gauges, as shown in Fig. 3.5, were installed on the column at 100mm from the bottom. Strain gauge Wheatstone bridges were configured with a half-bridge—two for measuring in the fore-and-aft direction and two for

measuring in the side-to-side direction.

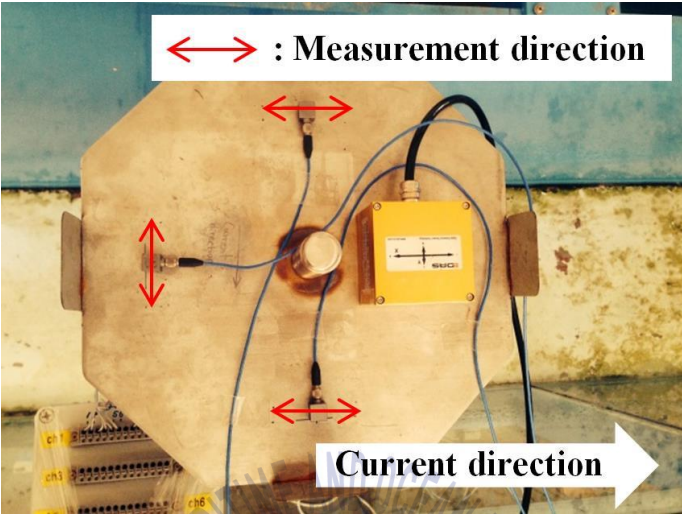
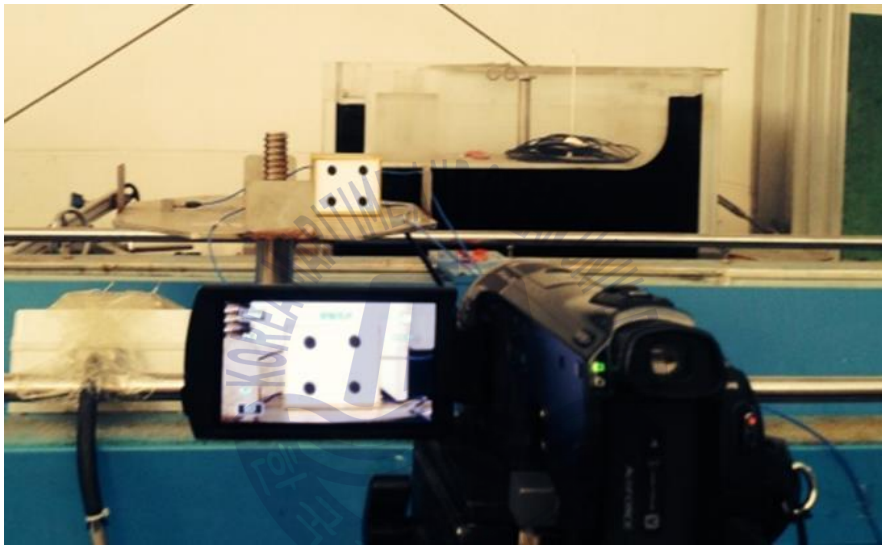


Fig. 3.4 Accelerometer location and measurement direction



Fig. 3.5 Location of strain gauge covered waterproof material

Temperature effect was ignored in the lab-scale experiment. Waterproof material was attached to prevent distortion of the strain response. The accelerometers and strain responses were obtained with a sampling rate of 300 Hz by MGCPlus (Operating manual), a data acquisition device (DAQ) produced by HBM, Inc. The real displacement was measured by recording the target on the top-plate using a camcorder as shown in Fig. 3.6.



**Fig. 3.6** Camcorder setup to measure real displacement

Although there are many methods to measure real displacements, it was difficult to affix this to the channel. The pump of the circulating water channel generated vibration on the experimental field, and there was much more vibration on the channel due to flow. This is why we could not install a LASER displacement meter on the channel to measure structural behavior in the current direction and used a camcorder instead to measure them from the outside of the water channel. Because the camcorder records at 30 frames

per second (fps), the first bending modal frequency of the lab-scale test structure (8.59 Hz) could be detected. To reduce the error and to improve the accuracy, the camcorder was installed as closely as possible to the lab-scale test structure. An image processing technique was employed to extract the displacement from the recording data (Yi et al., 2013c). The hydrometer was installed at least 5 m from the front of the lab-scale test structure to avoid flow interference.

### 3.3 Outline of the Lab-scale Experiment

The first lab-scale experiment is to observe the natural frequency with various water levels. Table 2 lists the order of the first lab-scale experiment.

**Table 2** Order of the first lab-scale experiment

Water level (mm)	Current velocity (m/s)	Boundary condition
From 0 to 800 at an interval of 100	0	Intact Case

In this experiment, the boundary condition is intact, which means that all bolts are fastened, as shown in Fig. 3.7. Tidal level changes on the Uldolmok Strait were simulated by water level changes in the circulating water channel. Changes in the water level can be changes of added mass. For this experiment, which was conducted without a current, the acceleration response was obtained from impact excitation. After the fast Fourier transform (FFT) analysis, the natural frequencies are obtained by reading the peak frequency

—i.e., peak-peaking method— in the frequency domain (Yi et al., 2004). However, the FFT resolution is not high enough to observe the variation of the natural frequencies. The eigensystem realization algorithm (ERA) method analyzed in the time domain was employed to allow more resolution in the frequency change compared with using FFT (Juang & Pappa, 1985). The second experiment was performed with the changing current velocity intact and two damage cases on the boundary connections. As shown in Fig. 3.7, these three cases are (1) Intact case; (2) Damage Case 1; and (3) Damage Case 2.

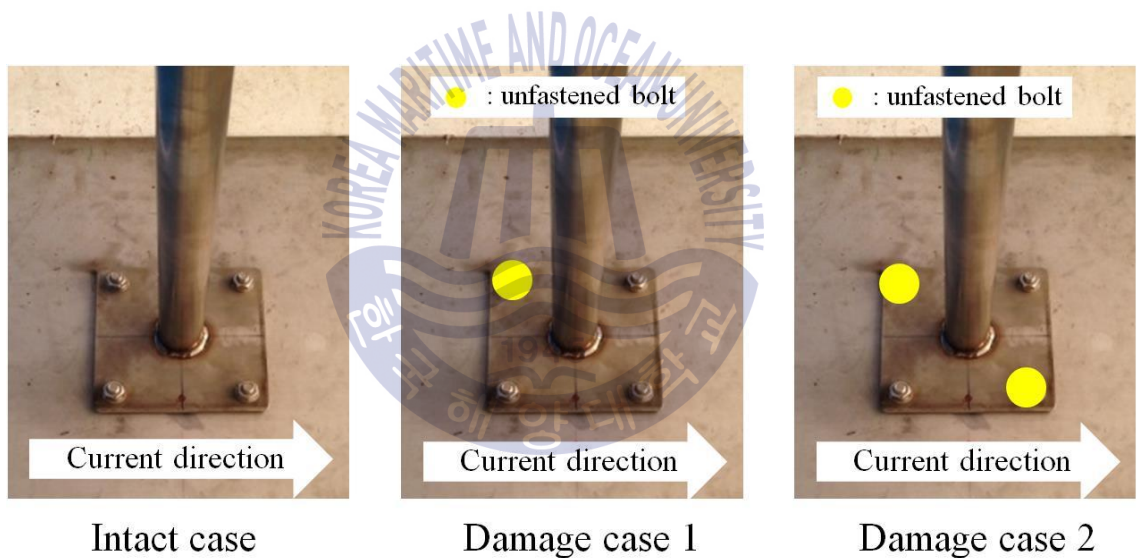


**Fig. 3.7** Definition of boundary conditions between the lab-scale test structure and the bottom

In Intact Case, the foundation of the lab-scale test structure and the bottom of the water channel are connected by fastening four bolts. Damage Case 1

is the condition with three fastened bolts, and Damage Case 2 is the condition with two fastened bolts. These are set diagonally. The order of the second experiment is given in Table 3. Because the lab-scale test structure was subjected to the current load, which causes ambient vibration, extra excitation was not needed. The natural frequencies are obtained using the former method of the first experiment. The acceleration responses were recorded with a sampling rate of 300 Hz.

**Table 3** Order of the second lab-scale experiment

Water level (mm)	Current velocity (m/s)	Boundary condition
350	0.39, 0.65, 0.92, 1.14, 1.31	Intact Case (four bolts)
350	0.39, 0.65, 0.92, 1.14, 1.31	Damage Case 1 (three bolts)
350	0.39, 0.65, 0.92, 1.14, 1.31	Damage Case 2 (two bolts)

### 3.4 Analysis of Experimental Results

#### 3.4.1 Added Mass Effect

Figure 3.8 shows the acceleration responses under impact excitation at a 500 mm water level, and Fig. 3.10 and 3.11 show the results for the first lab-scale experiment—the first and second bending modes in the fore-and-aft and side-to-side directions.

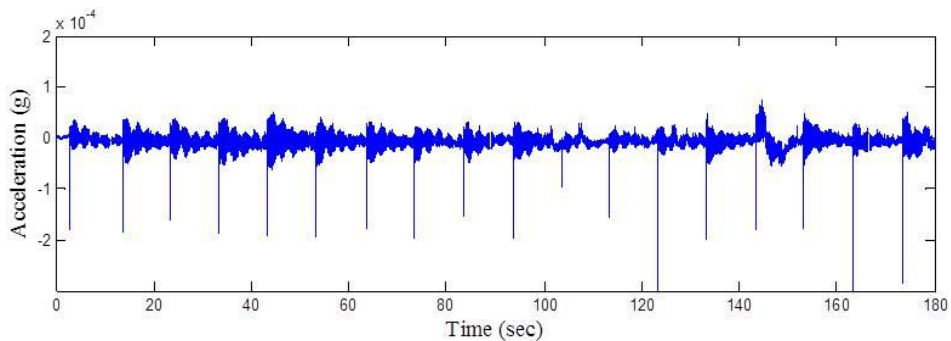


**Fig. 3.8** Acceleration time history response by impact excitation (500mm water level, fore-and-aft direction)

In the case of the first bending mode, theoretically, the natural frequency should decrease as the water level increases. However, as shown in Fig. 3.10 the first natural frequency in the fore-and-aft direction increased from 8.59 to 8.61 Hz by 0.02 Hz from 0 to 400 mm for the water level, and that in the side-to-side direction also increased from 9.09 to 9.11 Hz by 0.02 Hz. More discussion or additional tests may be needed. For more than a 400-mm water level, the natural frequencies for the first bending modes are, however, slightly reduced as the water level increases, but the change is very small—i.e., 0.58% from 8.61 to 8.56 Hz in the first modal frequency in the fore-and-aft direction and 0.76% from 9.11 to 9.04 Hz in the first modal frequency in the side-to-side direction. The second modal frequencies obviously decreased by 11.3%, as shown in Fig. 3.11. This is a reasonable result because the lower part of the cantilever beam has more modal sensitivities in case the second mode shape, as shown in Fig. 3.9. The reason

why there are differences between the first and second natural frequencies in the fore-and-aft direction from the side-to-side direction is due to asymmetry mass and stiffness of the lab-scale test structure. If structures have the perfect symmetry, the first and second natural frequencies would be the same.



(a) First bending mode shape (8.59 Hz)    (b) Second bending mode shape (99.73 Hz)

**Fig. 3.9** First and second bending mode shapes of the lab-scale test structure' s numerical model in dry condition

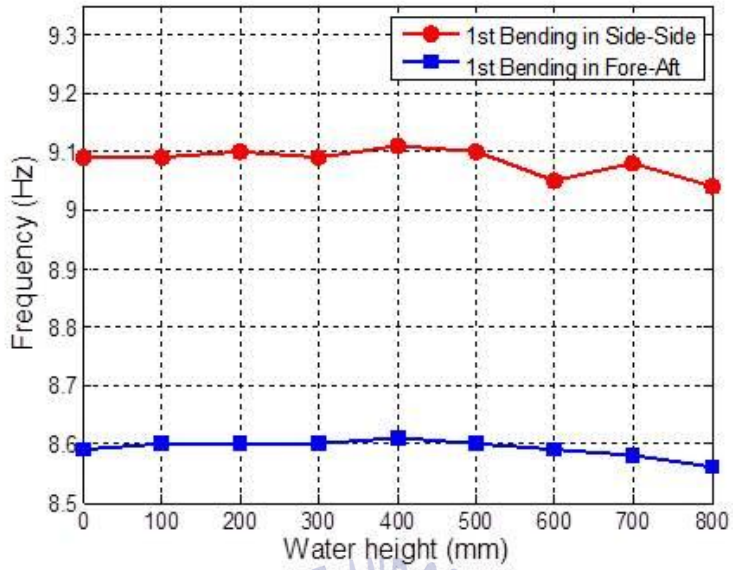


Fig. 3.10 The first bending modal frequencies in Side-side and Fore-aft direction as water level increases

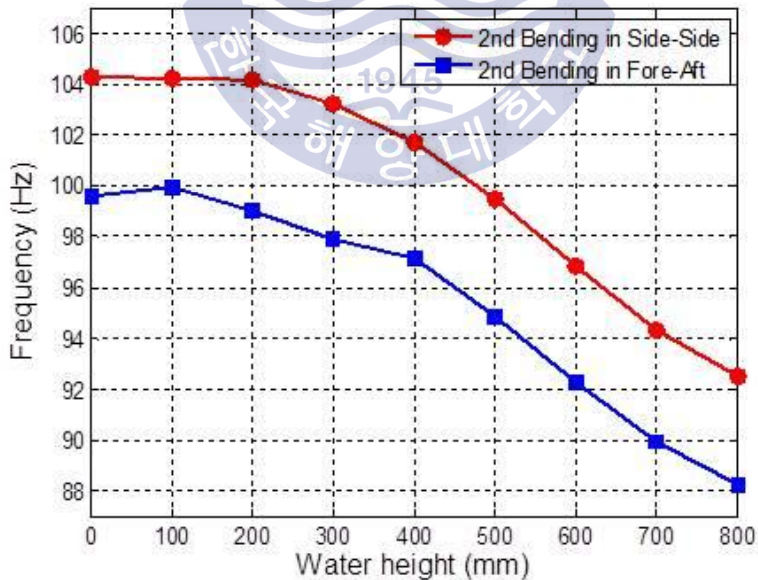
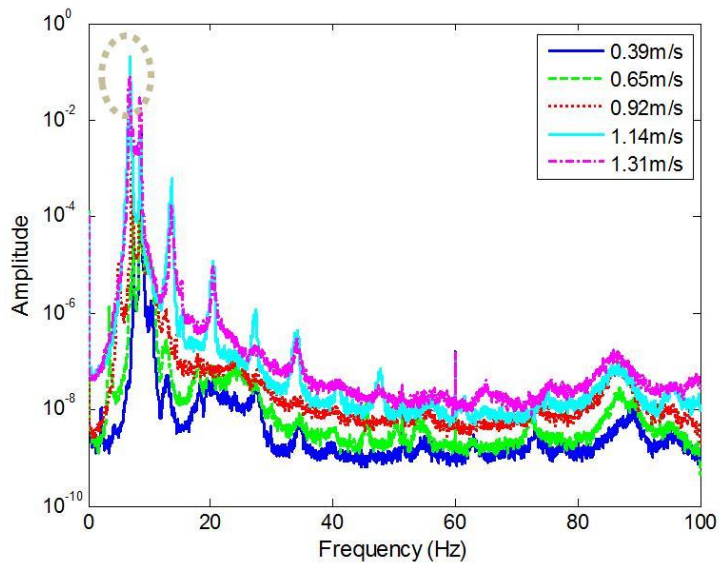


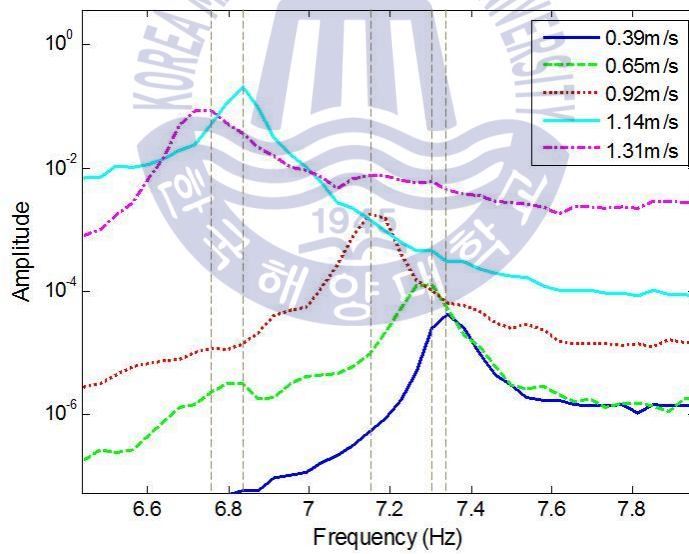
Fig. 3.11 The second bending modal frequencies in Side-side and Fore-aft direction as water level increases

### 3.4.2 Boundary Damage Effect from Current Velocity Change

Figure 3.12 shows the result of the second experiment in Damage Case 2. Power spectral density (PSD) data from the acceleration responses in every current velocity in Damage Case 2 are plotted in Fig. 3.12(a). The amplitude increases as the current velocity increases. Fig. 3.12(b) shows a partial extension of the circle marker in Fig. 3.12(a); this indicates the first bending modal frequency in the fore-and-aft direction. The peak frequencies gradually decrease with the increasing current velocity. The first natural frequencies of all boundary conditions are summarized in Fig. 3.13. In the cases of the intact condition and Damage Case 1, there were slight changes in the natural frequencies; however, the first natural frequency in Damage Case 2 decreased from 7.3 to 6.7 Hz—up to 8.25% with increasing water velocity. The reason why the natural frequencies decrease as the degree of the damage of the boundary connections becomes severe is due to reduction of stiffness in the boundary connections. Also, no effects of water velocity in Intact Case and Damage Case 1 indicate that the whole system of the lab-scale test structure is a linear system. However, if the damage of the boundary connection is severe such as in Damage Case 2, decreasing the natural frequency as the water velocity increases means that the lab-scale test structure may behave as a nonlinear system. Because the condition of the boundary connection is only changed in this experiment, the boundary connection is nonlinear. Therefore, the damage at the foundation is much more influential than the effect of the added mass associated with the tidal height in that the first frequency of the Uldolmok TCPP varies up to 16% in a day, and severe damage at the foundation can cause nonlinearity in the structural system.



(a) PSD data from acceleration in Damage Case 2



(b) Specific change in the first natural frequency

**Fig. 3.12** Result of the second lab-scale experiment in Damage Case 2 and its detail

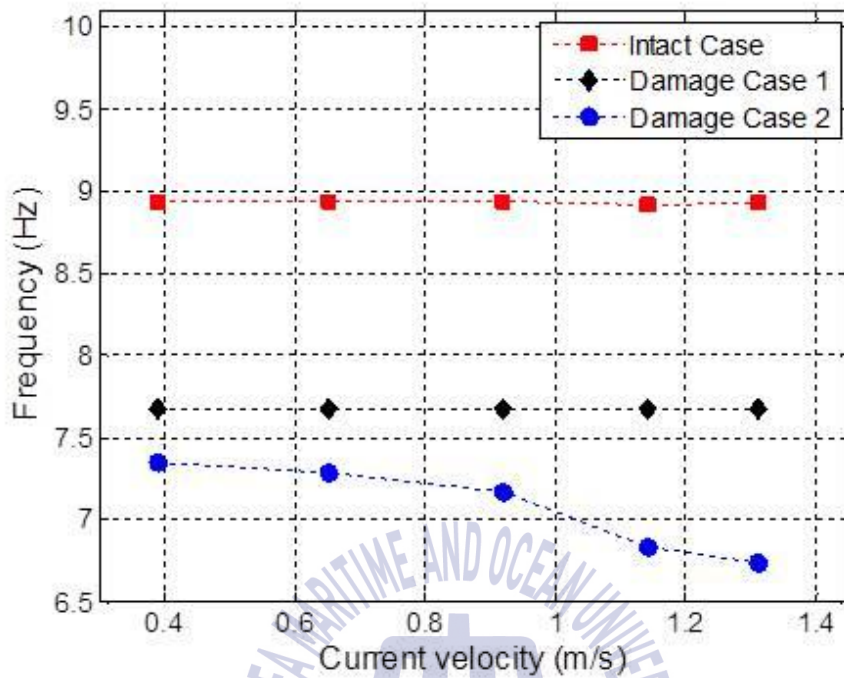


**Fig. 3.13** Changes in the first natural frequency in Intact Case, Damage Case 1, and Damage Case 2 as current velocity increases

Hence, it can be concluded that the natural frequency decreases more significantly as the damage at the foundation becomes severe. However, as for the stability of the whole structure, additional research is needed to evaluate quantitative damages.

### 3.4.3 Damage index ( $\beta$ )

Traditionally, efforts to easily and accurately determine the level of structural damage have been made by many damage indexes, such as the

natural frequency, modal shape, and modal curvature. The proposed damage index  $\beta$  in this study can be obtained by fusing data to estimate displacement, as shown in Eqs. (2.11), (2.16), and (2.17). Therefore, it is beneficial to detect the damage and estimate displacement simultaneously. The third lab-scale experiment to estimate displacement is carried out three times over three boundary conditions, and Fig. 3.14 shows each  $\beta$  value of Damage Cases 1 and 2.

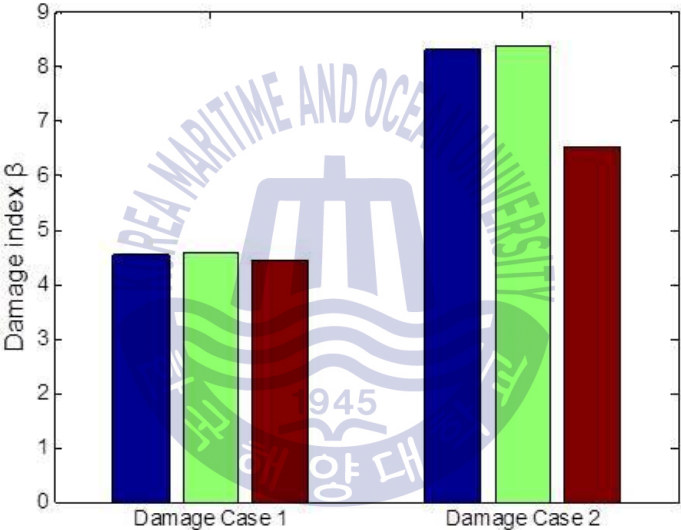


**Fig. 3.14** Damage index  $\beta$  for Damage Case 1 and Damage Case 2

The damage index  $\beta$  in Damage Case 1 has a larger value than Damage Case 2; i.e., the boundary damage becomes severe. The damage index  $\beta$  in Damage Case 1 has almost the same value. On the other hand, there is a difference between the maximum and minimum values of  $\beta$  by 1.88 in Damage Case 2; it is a large amount compared to that of Damage Case 1, by

0.134, as shown in Table 4. If more cases of Damage Case 2 are conducted, it could be discerned whether the third  $\beta$  of Damage Case 2 can be ignored as an experimental error by statistical analysis. Regarding this experiment result in itself, if  $\beta$  is monitored, we could determine whether the damage is ongoing. A large difference in  $\beta$  may mean that the structural system of Damage Case 2 is nonlinear.

**Table 4** Difference between maximum and minimum of  $\beta$  for Damage case 1 and Damage Case 2

Boundary condition	Intact Case	Damage Case 1	Damage Case 2
Difference between maximum and minimum of $\beta$	—	0.134	1.88

### 3.4.4 Displacement Estimation

As shown in Figs. 3.15–3.20, the results of the third experiment are plotted by two of every boundary condition. The real displacement from image processing and the estimated displacement from data fusion have similar trends. The pump and valve could generate ambient vibration; the pump was turned off during this experiment, and the pump has a large capacity. It maintains maximum current velocity by 1.31 m/s in the circulating water channel with a width of 600 mm and a height of 350 mm. It is possible for this vibration to be transmitted to the camcorder on the tripod and introduce with experimental errors because the maximum displacement of the lab-scale

test structure is very small—approximately 0.08 mm. In Fig. 3.16 in particular, it seems that the real displacement increased before the pump was turned off; however, this could be attributed to an experimental error (compared to the trends of other cases). We introduced two error factors, as shown in Eqs. (3.1) and (3.2):  $Err_1$  is the deviation of the maximum real (vision-based) and estimated displacements ( $u_{real,max}$  and  $u_{estimated,max}$ ), and  $Err_2$  is the root mean square error (RMSE) of the deviation between the real and the estimated displacements ( $u_{real}$  and  $u_{estimated}$ ). The  $Err_1$  and  $Err_2$  values of all cases are listed in Table 5. The two values decrease as the damage becomes severe; in other words, errors can be reduced when displacement is larger.

$$Err_1 = |u_{real,max} - u_{estimated,max}| \quad (3.1)$$

$$Err_2 = \frac{RMSE(u_{real} - u_{estimated})}{RMSE(u_{real})} \quad (3.2)$$

**Table 5**  $Err_1$  and  $Err_2$  of Intact Case, Damage Case 1, and Damage Case 2

Experimental cases	Intact Case		Damage Case 1		Damage Case 2	
	First try	Second try	First try	Second try	First try	Second try
$Err_1$	0.0151	0.0155	0.0083	0.0091	0.0068	0.0035
$Err_2$	0.4823	0.6113	0.2962	0.2608	0.2302	0.1029

To successfully perform experiments to measure the real displacement, we needed to find a method to accurately measure and fabricate the new structure having smaller stiffness, inducing large displacement, due to the fixed current velocity. Figures 3.15–3.20 and 3.21 show the accuracy of the

multimetric displacement estimation for quasi-static displacement and dynamic displacement, respectively. Therefore, this method was determined to be valid.

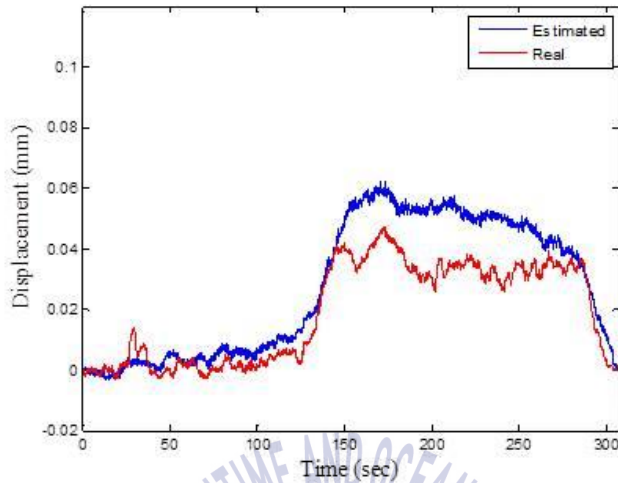


**Fig. 3.15** Estimated displacement at the top of the lab-scale test structure in Intact Case – first try

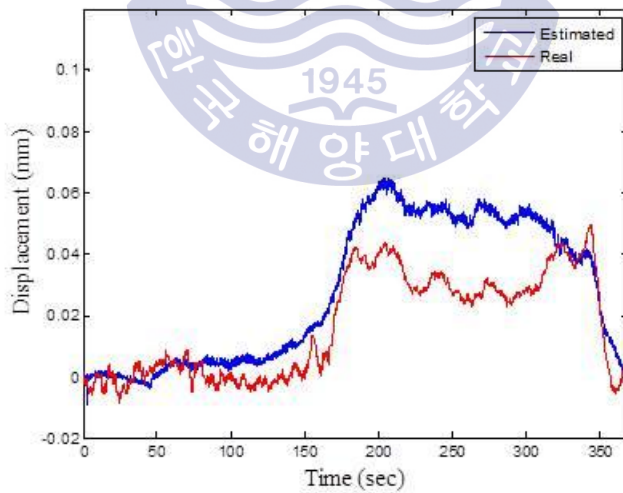


**Fig. 3.16** Estimated displacement at the top of the lab-scale test structure in Intact Case – second try

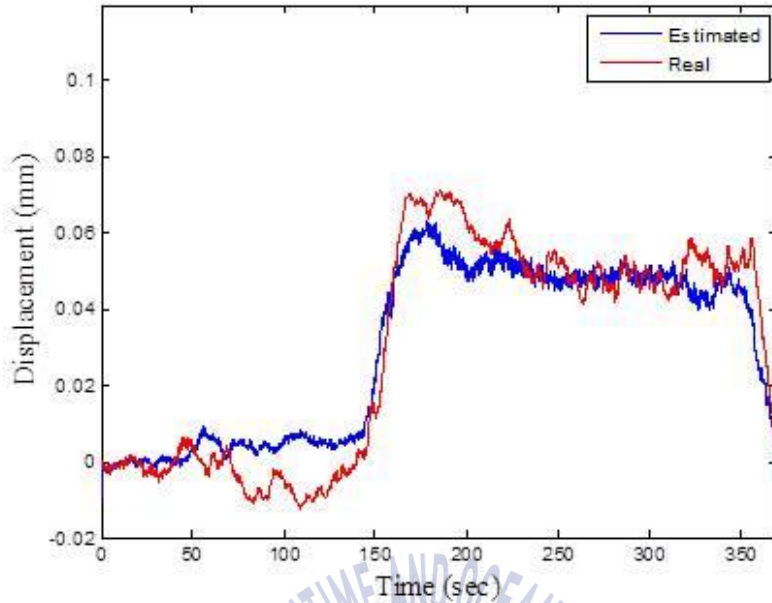


Fig. 3.17 Estimated displacement at the top of the lab-scale test structure in Damage Case 1 - first try

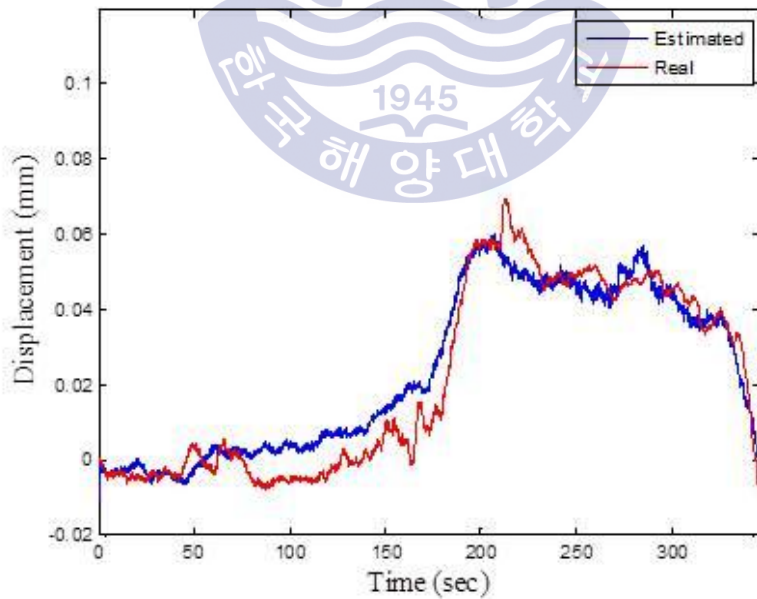


Fig. 3.18 Estimated displacement at the top of the lab-scale test structure in Damage Case 1 - second try

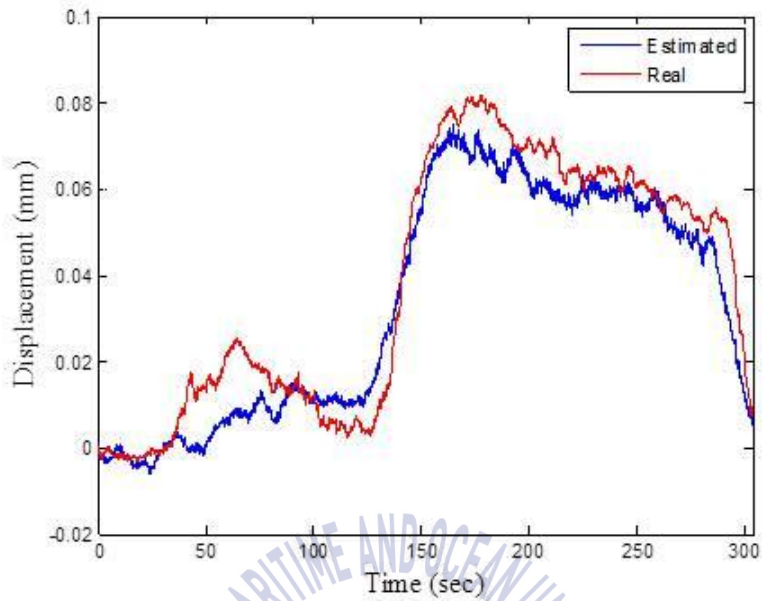


Fig. 3.19 Estimated displacement at the top of the lab-scale test structure in Damage Case 2 – first try

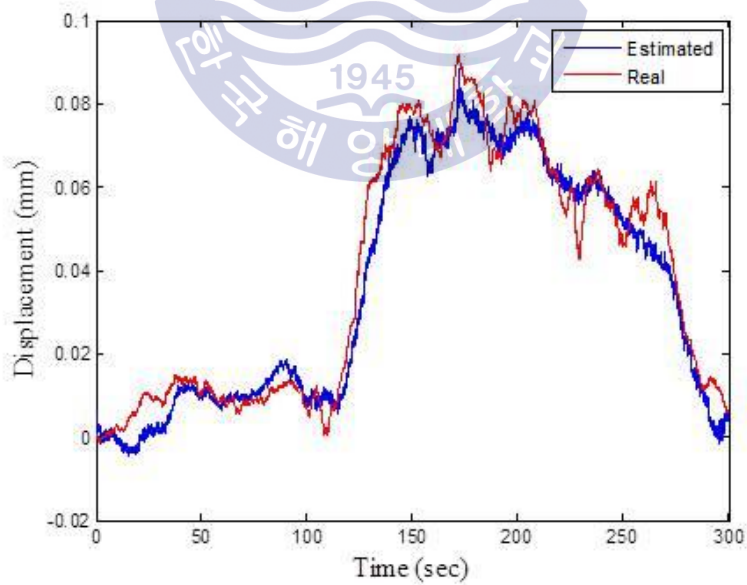


Fig. 3.20 Estimated displacement at the top of the lab-scale test structure in Damage Case 2 – second try

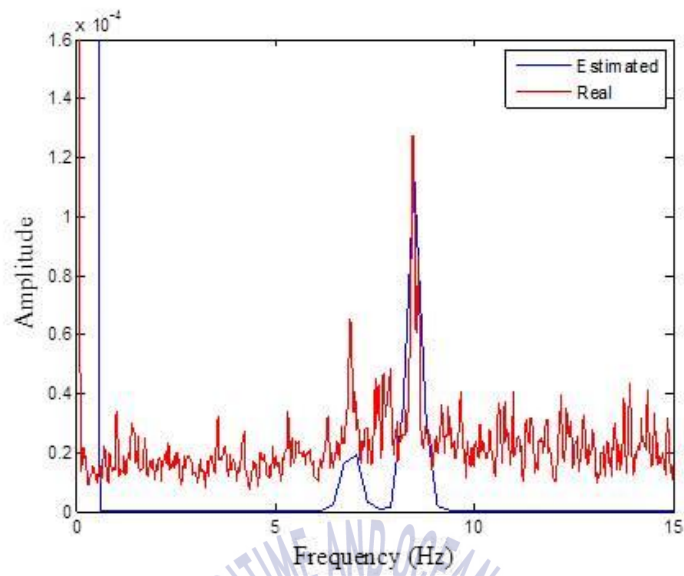


Fig. 3.21 PSD data for real and estimated displacement of Damage Case 2—first try



## Chapter 4.

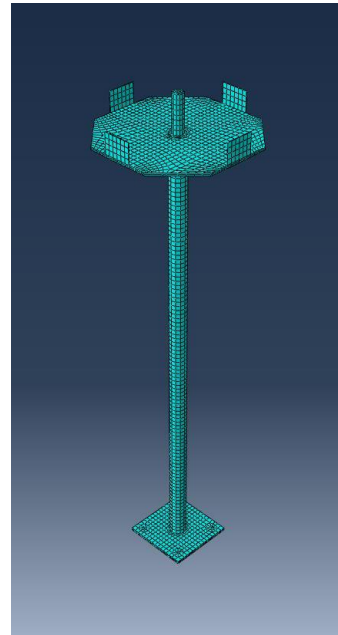
### VERIFICATION OF THE EXPERIMENT

#### 4.1 Outline of the Numerical Modeling

ABAQUS (ABAQUS 6.10.1, 2010), a commercial for finite element analysis code, was used to calculate the natural frequencies for verification of the experimental results. Figures 4.1(b) and (d) show the entire shape and the bottom shape of the elaborately simulated lab-scale test structure, respectively. As for the upper part of the lab-scale test structure, instead of simulating accelerometers, the weight of these was added to the upper part in modeling. Added mass was applied on the submerged part of the lab-scale test structure in the simulations to represent the water level increases in the experiment. The intact condition was simulated as shown in Fig. 4.1(d), where all bolts were fixed at four locations, satisfying a constraint condition in the longitudinal, fore-and-aft, and side-to-side directions. Damage Cases 1 and 2 were simulated by removing the constraint condition at the locations where the bolts are removed. The number of nodes and elements are 6,812 and 3,916, respectively, and the element type is a hexahedral solid. Because modal analysis for natural frequencies is theoretically not influenced by external forces, the effects of current velocity changes cannot be considered in the ABAQUS modeling.



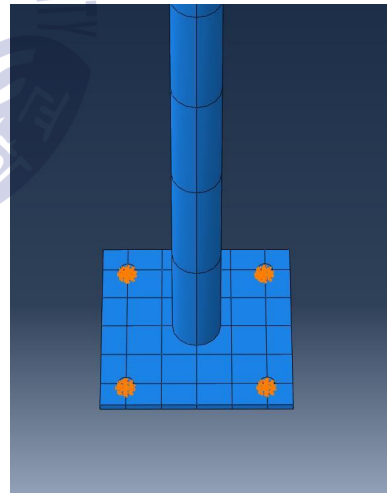
(a) Entire model—real



(b) Entire model—simulated



(c) Boundary condition—real

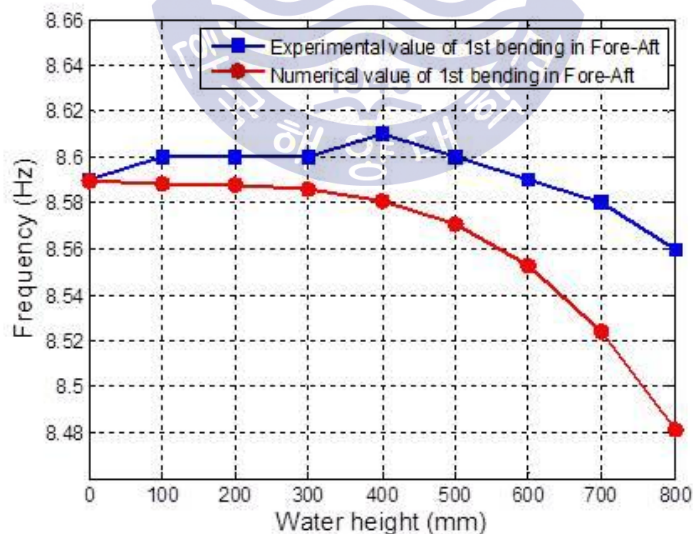


(d) Boundary condition—simulated

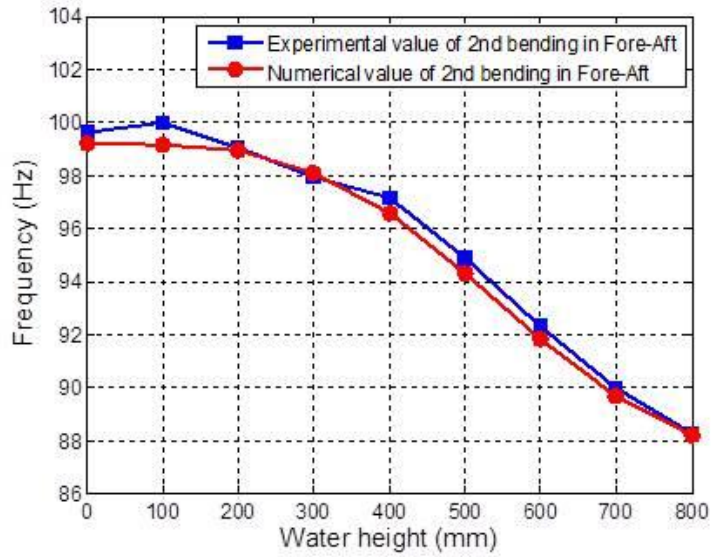
Fig. 4.1 Real and simulated numerical model of the lab-scale test structures

## 4.2 Added mass effect

As shown in Fig. 4.2, the experimental value of the first modal frequency in the fore-and-aft direction decreased by 0.6% from 8.61 to 8.56 Hz, while the numerical value decreased by 1.28%—more than double the experimental value from 8.59 to 8.48 Hz. However, in the case of the second bending mode in the fore-and-aft direction, the experimental and numerical values are very close to each other. Therefore, it can be confirmed that the previous equation for added mass—Eq. (2.2)—is correct for the second bending mode. However, in the case of the first bending mode, the particular constant is needed to fit the experimental and numerical values. This indicates that the added mass coefficient is dependent on each mode (i.e., frequency). We could find the correct added mass coefficient in the first bending mode by model updating.

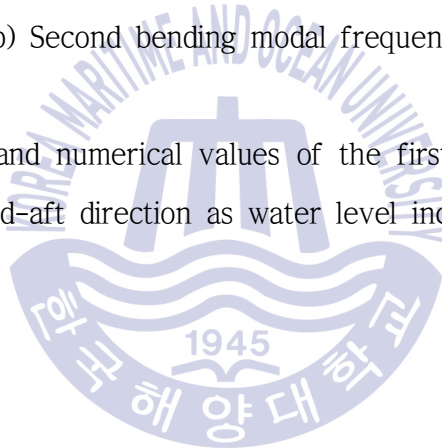


(a) First bending modal frequency



(b) Second bending modal frequency

Fig. 4.2 Experimental and numerical values of the first and second frequency in the fore-and-aft direction as water level increase



## Chapter 5

### CONCLUSION

#### 5.1 Conclusion

The motivation behind this paper came from the long-term observation of the identified natural frequencies of the Uldolmok tidal current power plant (TCPP). The natural frequencies of this structure under severe current environments have changed with the M2 (approximately 12 hours) and M4 (approximately 6 hours) tidal constituents. To study the main factor responsible, two lab-scale experiments were carried out using the lab-scale monopile-type test structure, simplified for the Uldolmok TCPP structure. We observed changes of the first natural frequency by controlling the main factors, including the water level, current velocity, and degree of damage in the boundary connections. In the first lab-scale experiment, the natural frequencies were extracted through the eigensystem realization algorithm (ERA) method for the acceleration response under impact excitation. In the second lab-scale experiment, the natural frequencies were calculated by the peak-picking method from the power spectral density (PSD) data. In addition, for the same purpose of SHM with the previous two experiments, another lab-scale experiment was conducted to verify the displacement estimation proposed by Park et al., (2013) using data fusion, and the degree of damage could be shown by damage index ( $\beta$ ), the normalized damage factor (NDF), which is from a scaling coefficient  $\alpha$ . Our concluding remarks are as follows:

- (1) Offshore structures consisting of cylinder members can be affected by

added mass, defined as Eq. (2.2). As shown in Fig. 4.2, however, this is not always applied on all modes; Eq. (2.2) is almost exact in the second bending mode; however, as for the first bending mode, the experimental decrease in the natural frequency was 46.9% of the numerical value. In other words, the added mass coefficient is dependent on the natural modes (i.e., frequency). Therefore, in monitoring vibration characteristics and assessing integrity of offshore structures, added mass effect should be accurately determined because natural frequency is the most fundamental factor in structural identification.

(2) Second lab-scale experiment indicated that the decrease of the natural frequencies depends on the degree of damage in the boundary connections under increase in current velocity. In the Intact Case and Damage Case 1 (degree of damage is not severe), there were slight changes in the natural frequencies; however, Damage Case 2 (degree of damage is severe) shows that stiffness decreases and nonlinearity increases as the degree of damage in the boundary connections becomes severe. In addition, in this situation, the natural frequencies decrease considerably as the current velocity increases. These results indicate that the degree of damage is an important component to influence the increase in nonlinearity and the dynamic characteristics of the structure.

(3) In the third lab-scale experiment, there were problems with accurately measuring the real displacement due to vibration from the pump and trouble with the installation of the LASER displacement meter with high accuracy. To accurately verify the estimated displacement, a measuring method for real (reference) displacement should be found. Nevertheless, the multimetric data fusion method proposed by Park et al., 2013 has sufficient validity in an

intact and damaged cantilever beam. The error in Intact Case was large because of too small amount of displacement; however, it can be recognized that the error in Damage Case 2, which has the largest displacement, decreased through the comparison of  $Err_1$  and  $Err_2$  of each boundary condition.

(4) We introduced damage index  $\beta$  in this study and compared Damage Cases 1 and 2 using this index. The degree of damage between the damage cases can be observed. The mean value of  $\beta$  in Damage Cases 1 and 2 were 4.44 and 6.51, respectively. This denotes the degree of damage. Three cases of Damage Case 1 had almost the same values of 0.134; however, the difference in Damage Case 2 was greater by 1.88. This indicates that Damage Case 1 is a linear system, but Damage Case 2 is a nonlinear system.

## 5.2 Future Study

In this study, big and long circulating water channel was used. Not only this water channel but others are connected with many segments. They had individual displacement and vibration when they start operation. Also, it was hard to fix the test structure because making holes to fix it is impossible; A lot of silicon was used in this study. That is why accuracy of this experiment was a little bit low. Next researcher who is going to carry out similar experiment should consider it. Future studies connected this study is suggested as below:

(1) Equations (2.2) and (2.4) indicate added mass and natural frequencies

considered added mass, respectively. It assumed that there was not water inside of submerged structural members. If there is, Eq. (2.4) should be change like Eq. (5.1).

$$f_i = \frac{1}{2\pi} \sqrt{\frac{K_i}{M_i + M_{ai} + M_w}} \quad (5.1)$$

where  $M_w$  is water mass inside of submerged structural members. After checking whether water is inside of submerged members of Uldolmok TCPP and lab-scale test structure, numerical and experimental study should be conducted to compare real phenomenon, which is frequencies changes, of Uldolmok TCPP with lab-scale test structure. Besides, numerical study is needed by applying real tidal height to numerical model for Uldolmok TCPP.

(2) It has many difficulties to construct offshore structures under harsh tidal current load, especially connecting main column and its foundation. To identify precisely, more similarly simulated experiment is recommended. In order word, lab-scale test structure connecting column and its foundation with concrete grout can be used. Before hardening it, current load would be subjected to test structure periodically and responses such as natural frequency and displacement can be observed as time goes on.

(3) The algorithm applied in displacement estimation covers the first natural frequency which is governing displacement. In the case of wind turbines, the main load on tower is thrust force on top of the tower. It absolutely lead this structure to vibrate like the first mode shape; however, governing load under other offshore structures such as tidal current power plant and wave power

plant is quite different from that of wind turbines. It means that other higher modes get involved in the vibration because excitation location is not on top of the structure. Therefore, modification of this algorithm is really needed. To improve the accuracy of displacement estimation, higher modes should be used in this algorithm.



## REFERENCE

Çelibi, M., 2000, GPS in dynamic monitoring of long-period structures. *Soil Dynamics and Earthquake Engineering*, 20(5), pp.477-483.

Cho, S.J., Sim, S.H., Park, J.W. & Lee, J.H., 2014, Extension of indirect displacement estimation method using acceleration and strain to various types of beam structures, *Smart Structures and Systems*, 14(4), pp.699-718.

Dassault Systemes Simulia Corp., 2010, Abaqus/CAE user' s manual, Version 6.10, Rhode Island, USA. <http://baribal.cyf-kr.edu.pl:2080/v6.10/index.html>.

DNV, 2010, Recommended Practice DNV-RP-C205 Environmental Conditions and Environmental Loads.

Fraenkel, P.L., 2007, Marine current turbines: pioneering the development of marine kinetic energy converters, *Journal of Power and Energy*, 221(2), pp.159-169

Salawu, O.S., 1997, Detection of structural damage through changes in frequency: A review, *Engineering Structures*, 19, pp.718-723.

Hallam, M.G., Heaf, N.J. & Wootton, L.R., 1977, Dynamics of Marine Structures: Methods of Calculating the Dynamic Response of Fixed Structures Subject to Wave and Current Action. (1st Edition), CIRIA UNDERWATER ENGINEER GROUP, London.

Han, S.H. et al., 2013, Evaluation of vertical axis turbine characteristics for

tidal current power plant based on in situ experiment, *Ocean Engineering*, 65, pp.83–89.

Huynh, T.C. et al., 2013, Simplified planar model for damage estimation of interlocked caisson system, *Smart Structures and Systems*, 12(3-4), pp.441–463.

Juang, J.N., & Pappa, R.S., 1985, An eigensystem realization algorithm for modal parameter identification and model reduction, *Journal of guidance, control, and dynamics*, 8(5), pp.620–627.

Jung, B.J., Park, J.W., Sim, S.H. & Yi, J.H., 2015, Issues in structural health monitoring for fixed-type offshore structures under harsh tidal environments, *Smart Structures and System*, 15(2), pp.335–353.

Kim, J.T. & Stubbs, N., 1995, Damage Detection in Offshore Jacket Structures from Limited Modal Information, *International Journal of Offshore and Polar Engineering*, 5(1), pp.58–66.

Lee, H.S., Hong, Y.H. & Park, H.W., 2010, Design of an FIR filter for the displacement reconstruction using measured acceleration in low-frequency dominant structures, *International Journal for Numerical Methods in Engineering*, 82(4), pp.403–434.

Lee, S.Y. et al., 2012, Vibration-based damage monitoring of harbor caisson structure with damaged foundation–structures interface, *Smart Structures and Systems*, 10(6), pp.517–546.

Lee, S.Y. et al., 2013, Vibration Characteristics of Gravity-Type Caisson Breakwater Structure with Water-Level Variation, *International Journal of Distributed Sensor Networks*.

Li, H.N. et al., 2014, Reviews on innovations and applications in structural

health monitoring for infrastructures, *Structural Monitoring and Maintenance*, 1(1), pp.1-45.

MGCPlus operating manual. Available online: <http://www.hbmdoc.com/fileadmin/mediapool/hbmdoc/technical/b0534.pdf> (accessed on 14 Jan. 2014)

Park, J.W., Sim, S.H. & Jung, H.J., 2013, Displacement estimation using multimetric data fusion, *IEEE/ASME Transactions on Mechatronics*, 18(6), pp.1675-1682.

Park, J.W., Sim, S.H., Yi, J.H. & Jung, H.J., 2014, Numerical Study of Temperature-robust Damage Factor based on Combination of an Accelerometer and an Inclinator for a Cantilever beam-type Structure, *Frontiers of Structural and Civil Engineering*, accepted.

Sedlar, D., Lozina, Z. & Vucina, D., 2011, Experimental Investigation of the Added Mass of the Cantilever Beam Partially Submerged in Water, *Technical Gazette*, 18(4), pp.589-594.

Weiner, E.O., Julyk, J.L. & Rezvani, M.A., 1994, Hydrodynamically Induced Loads on Components Submerged in High-level Waste Storage Tanks, Report of US Department of Energy.

Yi, J.H., Kim, J.H., Jeong, W.M. & Chae, J.W., 2013c, Field evaluation of optical-based three-dimensional dynamic motion measurement system with multiple targets for a floating structure, *Ocean Engineering*, 62, pp.140-151.

Yi, J.H. et al., 2013a, Flow-Turbine Interaction CFD Analysis for Performance Evaluation of Vertical Axis Tidal Current Turbines( I ), *Journal of Ocean Engineering and Technology*, 27(3), pp.67-72.

Yi, J.H., Park, J.S., Han, S.H. & Lee, K.S., 2013b, Modal Identification of a Jacket-type Offshore Structure Using Dynamic Tilt Responses and Investigation of Tidal Effects on Modal Properties, *Engineering Structures*, 49, pp.767-781.

Yi, J.H., Park, J.S., Park, J.S. & Lee, K.S., 2012, Long-Term Measurement of Static Strains of Jacket Type Offshore Structure under Severe Tidal Current Environments, *Korean Society of Civil Engineers*, 32(6A), pp.389-398.

Yi, J.H. & Yun, C.B., 2004, Comparative study on modal identification methods using output-only information, *Structural Engineering and Mechanics*, 17(3-4), pp.445-466.

